特 集 7
研 究 解 説

LES Analysis on Turbulent Flow past 2D Square Cylinder using Various Dynamic SGS Models

各種 Dynamic SGS モデルによる 2 次元角柱周辺流れの LES 解析

Shuzo MURAKAMI*, Satoru IIZUKA**, Akashi MOCHIDA** and Yoshihide TOMINAGA***
村 上 周 三・飯 塚 悟・持 田 灯・富 永 禎 秀

A turbulent vortex shedding flow past a two dimensional (2D) square cylinder at $Re=2.2\times10^4$ was analyzed by Large Eddy Simulation (LES) using various dynamic subgrid-scale (SGS) models. Here, 7 cases of computations were carried out using three different computational grids, two different grid systems and four different SGS models. Results from these computations were compared with those from the experiment by Lyn and Rodi. The Lagrangian Dynamic Mixed (LDM) model provided very good results in the four SGS models compared here. Furthermore, a method for stabilization by averaging over particle trajectories employed in the LDM model contributed to a remarkable improvement of computation stability.

1. Introduction

This paper reports on the results of Large Eddy Simulations (LES) of a turbulent vortex shedding flow past a two dimensional (2D) square cylinder at $Re=2.2\times10^4$ using various dynamic subgrid-scale (SGS) models [1-5]. The flowfield analyzed in this paper was one of the test cases for the LES Workshop of Flow past Bluff Bodies (Tengernsee workshop) held in Tengernsee, Germany, June 1995 [6] and also for the 2nd ERCOFTAC workshop on Direct and Large-Eddy Simulation held in Grenoble, France, September 1996.

The types of SGS models used are as follows ; the static type of conventional Smagorinsky model (S model, eqns.(1) and (2) in the Appendix (case 1)), the Dynamic Smagorinsky model (DS model, eqn.(6) in the Appendix (case 2)), the Dynamic Mixed model (DM model, eqn.(10) in the Appendix (case 3)) and the Lagrangian Dynamic Mixed model (LDM model, eqn.(16) in the Appendix (case 4)) (cf. Table 1).

Table 1 Computed cases

case	SGS model	grid	computational domain	number of grid point	h_w	average time (Note 1)
1	S (0.13,sf_μ)*1	colocated	20 (x_1) × 14 (x_2) × 2 (x_3)	104 (x_1) × 68 (x_2) × 10 (x_2) [grid A]	0.022	≈ 61
2	DS	colocated			0.022	≈ 15
3	DM	colocated			0.022	≈ 15
4	LDM	colocated			0.022	≈ 15
5	LDM	staggered			0.022	≈ 15
6	S (0.1,mf_μ)*1	colocated	20 (x_1) × 14 (x_2) × 4 (x_3)	107 (x_1) × 103 (x_2) × 14 (x_3) [grid B]	0.02	≈ 15
7	LDM	staggered		140 (x_1) × 103 (x_2) × 32 (x_3) [grid C]	0.02	≈ 61

h_w : the grid interval adjacent to the cylinder wall
*1 S (Cs, damping function*2)
*2 sf_μ : standard Van Driest damping (=1-exp(-x_n^+/25)), mf_μ : modified Van Driest damping (=(1-exp(-x_n^+/25)^3)$^{0.5}$)
Values are made dimensionless by the cylinder width, D, and the inflow velocity, U_0.

*Center for Development of Instrumentation Technology, Institute of Industrial Science, University of Tokyo
**Department of Building and Civil Engineering, Iustitute of Industrial Science, University of Tokyo
***Niigata Institute of Technology

2. Outline of computations

Table 1 lists 7 cases computed. Computations were carried out for three different computational grids (grids A-C), two different grid systems (colocated and staggered grids) and four different SGS models. Details of SGS models compared here are given in the Appendix. Preliminary computations were carried out on a relatively coarse grid (grid A) using four types of the SGS models in cases 1-4. The relative performance of these four SGS models was clarified by comparison with those given from the experiment by Lyn and Rodi [7]. As is described later, LDM model provided the best results.

A colocated grid was used in cases 1-4. In case 5, a computation using a staggered grid was carried out in order to assess the difference in prediction accuracy between colocated grid and staggered grid. In case 6, we carried out the computation with the same conditions as those of the computation by the University of Karlsruhe group for the LES Workshop of Flow past Bluff Bodies (Tegernsee workshop) [6] [Note 2]. Results of case 6 were compared with those of case 1. Finally, a computation using the LDM model was carried out with a grid spacing (grid C) which was finer than grid A used in cases 1-5 and grid B for case 6.

A second-order centered difference scheme was adopted for the spatial derivatives. For time advancement, the 2nd order Adams-Bashforth scheme was used for the convection terms and the Crank-Nicolson scheme for the diffusion terms. The interval for time advancement is 1.0×10^{-3} except for cases 2 and 3 (2.0×10^{-4} for cases 2 and 3) in non-dimensional time scale based on U_0 and D.

At the inflow boundary, the approach flow was set to be constant and uniform and no velocity fluctuations exist. A convective condition was used at the outflow boundary of the computational domain. Symmetry conditions were employed for the lateral boundaries, and periodicity conditions were imposed for the boundary planes perpendicular to the cylinder axis. For the boundary condition at the solid walls, Werner and Wengle's approach [8] was adopted [Note 3].

3. Comparison of various Dynamic SGS models with grid A (cases 1-4)

Firstly, the relative performance of various SGS models, i.e., S, DS, DM and LDM, are compared using grid A (cases 1-4, cf. Table 1).

Fig.1 shows the time-averaged velocity $\langle\bar{u}_1\rangle$ along the centerline. In front of the cylinder, the results are not influenced by the difference of the SGS models used, but there are fairly large differences in the wake region. Case 1 (S model) underestimates the length of the reverse flow region considerably. Both cases 2 (DS model) and 3 (DM model) show good agreement with the experiment than does S model, and there is little difference between the results obtained with these two types of dynamic SGS models in the region of $0.5<x_1<1.5$. Further downstream ($x_1>1.5$), case 3 (DM model) seems to give more reasonable result than does case 2 (DS model).

Fig.2 compares the time-averaged velocity $\langle\bar{u}_1\rangle$ along the centerline between case 3 (DM model) and case 4 (LDM model). In the LDM model, the model coefficient C ($C=Cs^2$) is calculated using the averaged quantities along the path line following the approach developed by Meneveau et al. [5] (eqns.(12)-(17) in the Appendix).

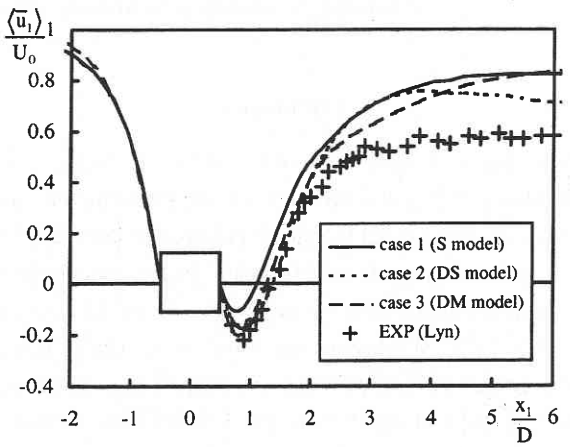

Fig. 1 Comparison of the time-averaged velocity $\langle\bar{u}_1\rangle$ along the centerline for S, DS and DM models

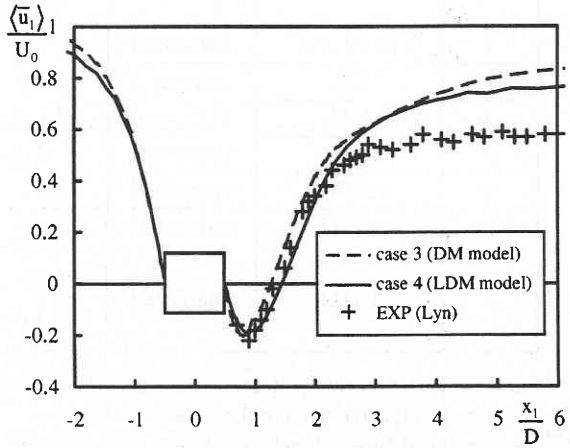

Fig. 2 Comparison of the time-averaged velocity $\langle\bar{u}_1\rangle$ along the centerline for DM and LDM models

Although both results show good agreement with the experiment, case 4 (LDM model) provides more accurate result than case 3 (DM model). The LDM model seems to provide the best result in these four SGS models compared. Furthermore, the use of LDM model contributes to a remarkable improvement of calculation stability as shown in Fig. 3. Consequently, CPU time was reduced by 33% in comparison with DM model.

4. Influence of difference in grid spacings (comparison between case 1 and case 6)

The conditions for computation, i.e., the grid spacing, SGS model, etc., employed in case 6 is almost the same as those in the computation by the University of Karlsruhe group presented at the LES Workshop of Flow past Bluff Bodies [6].

The result of case 6 is compared with case 1 in Fig. 4. The spatial oscillation of velocity is observed in the region of $x_1 > 2$ in case 6, while this oscillation does not appear in the result of case 1. As described in Note 4, this difference is mainly caused by the difference in the grid spacings for both cases. The spacing of grid B (case 6) in the streamwise (x_1) direction is coarser than that of grid A (case 1) in the region behind the cylinder ($x_1 > 1$). The spacing in the spanwise (x_3) direction of grid B (case 6) is also coarser than that of grid A (case 1) for the whole domain. By these coarse spacings of grid B, the spatial oscillation of velocity was caused in case 6 in the region behind the cylinder as is indicated in Fig. 4. On the other hand, the resolution of grid B in x1 and x_2 directions is finer than that of grid A in the vicinity of the cylinder wall ($-1 < x_1 < 1$). Hence, the computation with grid B provided more accurate results in the vicinity of the cylinder wall in comparison with the results using grid A. Considering these points, a new grid (grid C) was designed. The resolution of grid C in x_1 and x_2 directions is almost the same as that of grid B in the vicinity of the cylinder wall, but much finer than that of grid B in the region behind the cylinder. In this region, the resolution of grid C in x_1 direction becomes identical to that of grid A. Furthermore, the grid spacing in the spanwise (x_3) direction is much finer in grid C than those in grid A and grid B.

5. Performance of LDM model with grid C (case 7)

Hereafter, results of a computation using LDM model with grid C (case 7) are shown. In this case, the staggered grid was used (cf. Note 5). Integral parameters are compared in Table 2. The statistical quantities were

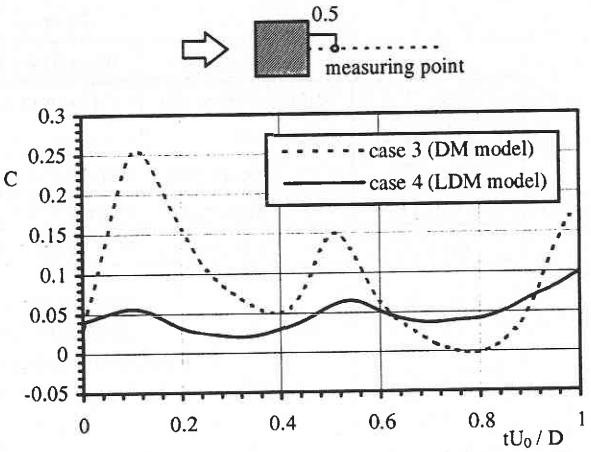

Fig. 3 Comparison of the time-history of model coefficient C between DM and LDM models

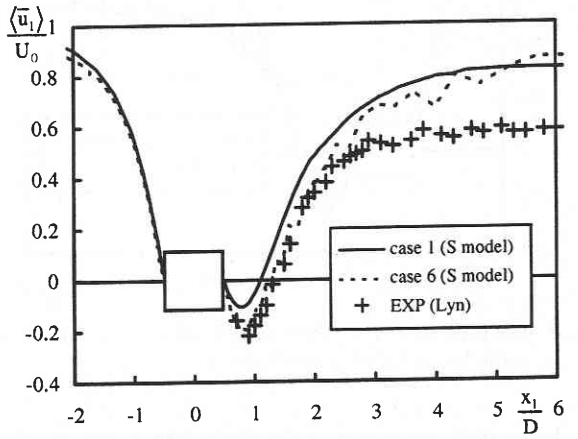

Fig. 4 Comparison of the time-averaged velocity $\langle \bar{u}_1 \rangle$ along the centerline between cases 1 and 6

determined by using the time-history of predicted flowfields during 8 vortex shedding periods for this case. The correspondence between the results of case 7 and experiments is satisfactory except for the value of C_{Drms}. Fig.5 compares the time-averaged velocity $\langle \bar{u}_1 \rangle$ along centerline. The result of case 7 reproduced the velocity distribution in the reverse flow region behind the cylinder accurately.

6. Conclusions

(1) Dynamic SGS models provide much more accurate predictions of the sizes of the reverse flow region behind the cylinder than does the static type of conventional Smagorinsky model (S model).

(2) A method for stabilization by averaging over particle trajectories employed in LDM model can contribute to remarkable improvement of calculation stability. Within

Table 2 Integral parameters

	$L_1 \times L_2 \times L_3$	$N_1 \times N_2 \times N_3$	h_w	St	$<C_D>$	C_{Drms}	C_{Lrms}
case 7 (LDM model)	$20D \times 14D \times 4D$	$140 \times 103 \times 32$	0.02	0.131	2.05	0.12	1.39
Lyn [7]	Experiment	$(Re=2.2 \times 10^4)$		0.132	2.1	—	—
Vickey [12]	Experiment	$(Re=1 \times 10^5)$		—	2.05	—	1.32
Lee [13]	Experiment	$(Re=1.76 \times 10^5)$		—	2.05	0.23	1.22

L_i : computational domain in x_i direction (i=1,2,3)
N_i : mesh resolution in x_i direction
St : Strouhal number
C_D : drag coefficient
C_L : lift coefficient
h_w : the grid interval in the normal direction adjacent to the cylinder wall

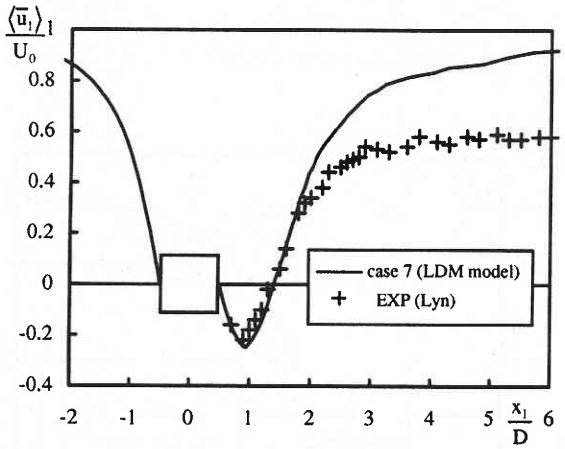

Fig. 5 Comparison of the time-averaged velocity $\langle \bar{u}_1 \rangle$ along the centerline of LDM model (case 7)

the experiences of our group, the LDM model seems to be most suited for the analysis of flowfield around a cylinder, since it provides good calculation stabilities and also good prediction accuracy.

Appendix SGS models compared

In the Smagorinsky model, the anisotropic part of the SGS stress τ_{ij} is modeled as follows:

$$\tau_{ij} - \frac{1}{3}\delta_{ij}\tau_{kk} = -2C\bar{\Delta}^2 |\bar{S}| \bar{S}_{ij} = -2\nu_{SGS}\bar{S}_{ij} \quad (1)$$

where SGS viscosity ν_{SGS} is

$$\nu_{SGS} = C\bar{\Delta}^2 |\bar{S}| \qquad (C = Cs^2) \quad (2)$$

Here, $\bar{\bullet}$ (denotes the grid-filtered values and $\bar{\Delta}$ is the width of the grid-filter, $\bar{S}_{ij}$ is the resolved-scale strain rate tensor,

$$\bar{S}_{ij} = \frac{1}{2}\left(\frac{\partial \bar{u}_i}{\partial x_j} + \frac{\partial \bar{u}_j}{\partial x_i}\right), \quad |\bar{S}| = (2\bar{S}_{ij}\bar{S}_{ij})^{1/2} \quad (3)$$

In S model (cases 1 and 6), C is treated as a constant. The value of 0.0169 and 0.01 were selected for cases 1 and 6, respectively. These values correspond to 0.13 and 0.1 of the so-called Smagorinsky constant Cs (cf. Table 1). $\bar{\Delta}$ is multiplied by the Van Driest type wall damping function f_μ, 1-exp $(-x_n^+/25)$ in case 1 and mf_μ, $\{1 - \exp(-x_n^+/25)^3\}^{0.5}$ in case 6 in order to account for the near wall effect in S model, while f_μ is not necessary in dynamic SGS models.

In dynamic SGS models, the model coefficient C is determined dynamically. Following Germano et al.[1], a test filter (denoted as $\hat{\bullet}$ in this paper) is introduced to derive an expression for C. The width of test-filter is taken to be twice the width of grid-filter. Germano et al. defined the resolved turbulent stress as follows:

$$\pounds_{ij} = \widehat{\bar{u}_i\bar{u}_j} - \hat{\bar{u}}_i\hat{\bar{u}}_j \quad (4)$$

$\pounds_{ij}$ can be related to the SGS stress τ_{ij} and the subtest-scale stress $T_{ij} = \widehat{\bar{u}_i\bar{u}_j} - \hat{\bar{u}}_i\hat{\bar{u}}_j$ by

$$\pounds_{ij} = T_{ij} - \hat{\tau}_{ij} \quad (5)$$

DS model (case 2) employs the dynamic procedure using a least square method proposed by Lilly [2] to determine the coefficient C:

$$C(\vec{x}, t) = -\frac{1}{2}\frac{\pounds_{ij}M_{ij}}{M_{kl}^2} \quad (6)$$

where $M_{ij} = \hat{\bar{\Delta}}^2 |\hat{\bar{S}}| \hat{\bar{S}}_{ij} - \widehat{\bar{\Delta}^2 |\bar{S}| \bar{S}_{ij}}$ (7)

In DM model (case 3), a linear combination of the dynamic Smagorinsky model and the scale similarity model is adopted [4, 14]. In DM model, anisotropic part of (τ_{ij} is expressed as [4, 14]:

$$\tau_{ij} - \frac{1}{3}\delta_{ij}\tau_{kk} = -2\nu_{SGS}\bar{S}_{ij} + B_{ij} - \frac{1}{3}\delta_{ij}B_{kk} \quad (8)$$

where $B_{ij} = \overline{\bar{u}_i\bar{u}_j} - \bar{u}_i\bar{u}_j$ (9)

The first and the second terms in the right-hand of eqn.(8) derive from the Smagorinsky and the scale similarity models respectively.

Here, C is determined by

$$C(\vec{x},t) = -\frac{1}{2}\frac{M_{ij}(\pounds_{ij} - H_{ij})}{M_{kl}^2} \quad (10)$$

where H_{ij} is the term originated from the scale similarity model. H_{ij} is written as [4];

$$H_{ij} = \widehat{\hat{\bar{u}}_i\hat{\bar{u}}_j} - \hat{\bar{u}}_i\hat{\bar{u}}_j - (\widehat{\bar{u}_i\bar{u}_j} - \bar{u}_i\bar{u}_j) \quad (11)$$

The value of C obtained from eqns.(6) and (10) can be either positive or negative. A negative value of C implies a locally negative value of eddy-viscosity which causes the numerical instability. In cases 2 and 3, we set the coefficient C equal to be zero wherever C is estimated to be negative (clipping procedure).

Previous authors have used an averaging over homogeneous directions to avoid the numerical instability (Germano et al.[1], Akselvoll et al.[15], Zang et al.[3]). The disadvantages of this treatment is that the plane-averaging can only be applied to flowfields that have a homogeneous direction. This treatment cannot be applied to three-dimensional flowfields such as a flow around a cube. Thus, this treatment excludes the application of LES to more challenging flows of engineering interest. In Lagrangian Dynamic Smagorinsky model (LDS model), the model coefficient C is calculated following the approach developed by Meneveau et al.[5] in which the residual in eqn.(5) is minimized along fluid trajectories rather than flow homogeneous directions, resulting in an expression for the model coefficient;

$$C(\vec{x},t) = -\frac{1}{2}\frac{I_{LM}}{I_{MM}} \quad (12)$$

The numerator and denominator of eqn.(12) are obtained using a simple time discretization, resulting in

$$I_{LM}^{n+1}(\vec{x}) = H\{\varepsilon\pounds_{ij}M_{ij}^{n+1}(\vec{x}) + (1-\varepsilon)I_{LM}^{n}(\vec{x} - \bar{u}_i^{n}\Delta t)\} \quad (13)$$

$$I_{LM}^{n+1}(\vec{x}) = \varepsilon M_{ij}M_{ij}^{n+1}(\vec{x}) + (1-\varepsilon)I_{MM}^{n}(\vec{x} - \bar{u}_i^{n}\Delta t)\} \quad (14)$$

where H{x} is the ramp function (H{x} = x if x>0 and zero otherwise), and

$$\varepsilon = \frac{\Delta t / T^n}{(1 + \Delta t / T^n)} \quad (15)$$

The technique of Lagrangian averaging can be easily added to the Dynamic Mixed model. We call it LDM model.

$$C(\vec{x},t) = \frac{1}{2}\frac{I_{LM} - I_{HM}}{I_{MM}} \quad (16)$$

where

$$I_{HM}^{n+1}(\vec{x}) = \varepsilon H_{ij}M_{ij}^{n+1}(\vec{x}) + (1-\varepsilon)I_{HM}^{n}(\vec{x} - \bar{u}_i^{n}\Delta t) \quad (17)$$

LDM model was used in cases 4, 5 and 7 in Table 1.

The time-scale T in eqn.(15) is defined as $T=\alpha n$ ($n=\bar{\Delta}I_{LM}^{-1/4}$). Meneveau et al.[5] recommend a value of 2 for a based on the filtered DNS data of isotropic turbulence. Within the experiences of our group, this value of 2 was not optimum for α (T=2n) for flow around a bluff body. Here, the value of 0.2 was selected for α (T=0.2n) in cases 4, 5 and 7 as a result of numerical experiments.

Note 1

The time-averaged values were determined by the time-averaging over 8 vortex shedding periods (61 in the non-dimensional time scale) in case 1 as well as by averaging over the spanwise direction.

Fig.6 compares the time-averaged velocity determined by time-averaging over 2 shedding periods with that averaged over 8 shedding periods for case 1 (S model). The difference between values based on these two different averaging time is very small as far as time-averaged velocity is concerned. Thus, the averaging time for time-averaged values was reduced to 2 vortex shedding periods (15 in the non-dimensional time scale) in cases 2-6.

Note 2

This computation by Karlsruhe group was recommended as a reference for the test case for the 2nd ERCOFTAC workshop held in Grenoble, 1996.

Note 3

In Werner and Wengle's approach [8], a linear or 1/7 power-law distribution of the instantaneous velocity is assumed :

$$\frac{\bar{u}}{u^*} = x_n^+ \qquad (x_n^+ \leq 11.81), \tag{18}$$

$$\frac{\bar{u}}{u^*} = 8.3x_n^{+1/7} \qquad (x_n^+ > 11.81), \tag{19}$$

This wall function becomes identical to the no-slip boundary condition when $x_n^+ \leq 11.81$. Fig.7 illustrates the distribution of time-averaged values of x_n^+ of the grid points adjacent to the cylinder walls. In most areas, the value of is lower than 11.81. Thus the linear-law, i.e., the no-slip boundary condition, is applied in these areas. At corner areas, the value of x_n^+ slightly exceeds 11.81.

Note 4

As shown in Table 1, four factors, i.e., grid spacings, values of Cs, wall damping functions and sizes of computational domain in spanwise direction, are different between cases 1 and 6. In the earlier research by our group (Murakami et al. [9]), the influence of the Cs value and the size of computational domain was examined. In that study, computations were carried out for two different values of Cs (0.13 and 0.1 adopted in cases 1 value and 6 respectively) with grid A. As shown in [9], the difference between the results of these two cases was very small. Furthermore, two computations were carried out and compared for two sizes of different computational domain in the spanwise direction, 2D and 4D in [9]. Regarding the time-averaged velocity , the result of the case with a larger computational domain (4D) provided a slightly smaller reverse flow region behind the cylinder. However, we noted that there were no outstanding differences for each computational domain size.

We have also carried out another computation (case 6') in which only the damping function was changed from $mf_\mu(=(1 - \exp(-x_n^+/25)^3)^{0.5})$ adopted in case 6 to the function used in case 1 (f_μ = 1-exp ($- x_n^+/25$)). Through the comparison between the results of cases 6 and 6', it was confirmed that the results were not much affected by the difference in the forms of wall damping functions.

The rest of different factors between cases 1 and 6 is grid spacing. We consider that the difference in the grid spacings is the main factor for the differences between the results of both cases.

Note 5 Comparison between colocated grid and staggered grid

A colocated grid (Rhie and Chow [10]) was used for cases 1-4 and 6. However, recently it was reported that the result based on staggered grid provides more accurate prediction

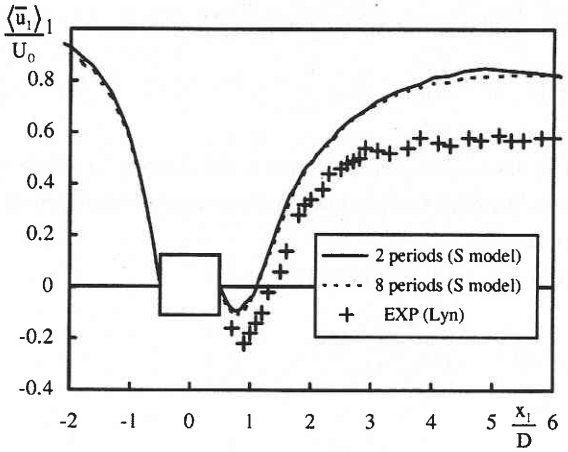

Fig. 6 Comparison of the time-averaged velocity $\langle \bar{u}_1 \rangle$ along the centerline determined by time averaging over 2 shedding periods and 8 shedding periods

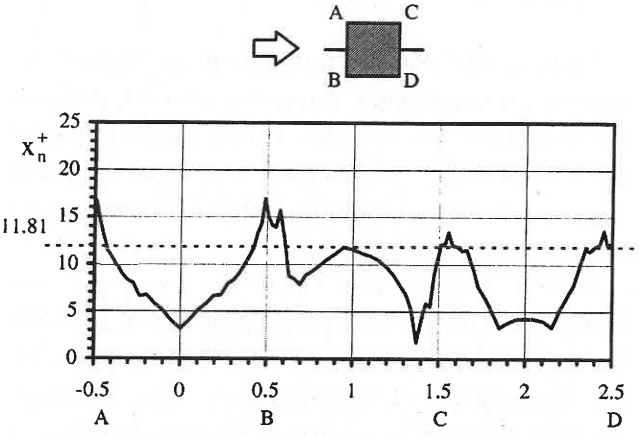

Fig. 7 Distribution of time-averaged values of x_n^+ (case 7)

than that based on colocated grid in a LES computation of channel flow, because the result based on colocated grid includes some numerical errors (Ooka et al. [11]).

In this study, we compared the result based on colocated grid (case 4) with that based on staggered grid (case 5). As for the time-averaged velocity $\langle \bar{u}_1 \rangle$, both results are almost the same, but case 5 is slightly better (figures are omitted here). So we used staggered grid for case 7.

Nomenclature

x_i	: three components of the spatial coordinate (i = 1,2,3 : streamwise, lateral, spanwise)
u_i	: three components of the velocity vector
f	: instantaneous value of a quantity
$\bar{f}$	: filtered value of f
$<f>$	: time averaged value of f
x_n	: distance from the wall

$x_n^+ = x_n u^*/\nu$, u^*: friction velocity

Re : Reynolds number, $Re = U_0 D/\nu$

D : width of the square cylinder

U_0 : $<u_1>$ value at inflow of computational domain

When values are made dimensionless, the representative length scale D, velocity scale U_0 and air density ρ are used.

(Manuscript received, October 24, 1996)

References

1) Germano,M., U. Piomelli, P. Moin and W.H. Cabot : A dynamic subgrid-scale eddy viscosity model, Phys. Fluids, A3, 1760 (1991).
2) Lilly, D.K., A proposed modification of the Germano subgrid-scale closure method, Phys. Fluids A4, 633 (1992).
3) Zang,Y., R.L. Street and J.R. Koseff : A dynamic mixed subgrid-scale model and its application to turbulent recirculating flows, Phys. Fluids A5(12) (1993).
4) Vreman,B., B.Geurts and H.Kuerten, On the formulation of the dynamic mixed subgrid-scale model, Phys. Fluids 6(12), pp. 4057-4059 (1994).
5) Meneveau,C., T.S.Lund and W.Cabot, A lagrangian dynamic subgrid-scale model of turbulence, Proceedings of the Summer Program 1994, Center for Turbulence Research, pp. 2746-2757 (1991).
6) LES workshop of Flows past Bluff Bodies, June 26-28 Rottach-Egern, Tegernsee, Germany, organized by W.Rodi and J.H. Ferziger (1995).
7) Lyn,D.A. and W.Rodi, The flapping shear layer formed by flow separation from the forward corner of a square cylinder, J. Fluid Mech., vol. 267, pp. 353-376 (1994).
8) Werner, H. and H. Wengle, Large-eddy simulation of turbulent flow over and around a cube in a plate channel, 8th Symp. on Turbulent Shear Flows 19-4 (1991).
9) Murakami, S., W.Rodi, A. Mochida and S. Sakamoto, Large eddy simulation of turbulent vortex shedding flow past 2D square cylinders, in: Proc. Symp. on Engineering applications of large eddy simulations (FED-Vol. 162). ASME p.113 (1991).
10) Rhie, C.M. and W.L. Chow, Numerical study of the turbulent flow past an airfoil with trailing edge separation, AIAA Journal, vol. 21, No.11 (1983).
11) Ooka, R., S. Murakami and A. Mochida, Study on conservation property of kinetic energy of LES with colocated grid, submitted to International Journal of Numerical Method in Fluids (1996).
12) Vickery, B.J., Fluctuating lift and drag on a long cylinder of square cross section in a smooth and a turbulent stream, J. Fluid Mech. 25, p. 481 (1975).
13) Lee, B.E., The effect of turbulence on the surface pressure field of square prisms, J. Fluid Mech. 69, p. 263 (1975).
14) Bardina, J., J.H. Ferziger and W.C. Reynolds, Improved Subgrid-scale models for Large-Eddy Simulation, AIAA paper-80 (1981).
15) Akselvoll, K., and P. Moin, Large eddy simulation of a backward facing step flow, Eng. Turbulence Modelling and Experiments 2 pp. 303-313 (1993).